Mineralogical and Geochemical Vectors within Advanced Argillic-Altered Rocks of North-Central British Columbia (NTS 094E/02, 15, 104I/05)

F. Bouzari, MDRU - Mineral Deposit Research Unit, The University of British Columbia, Vancouver, British Columbia, fbouzari@eoas.ubc.ca

R.G. Lee, MDRU - Mineral Deposit Research Unit, The University of British Columbia, Vancouver, British Columbia

C.J.R. Hart, MDRU - Mineral Deposit Research Unit, The University of British Columbia, Vancouver, British Columbia

B.I. van Straaten, British Columbia Geological Survey, British Columbia Ministry of Energy, Mines and Low Carbon Innovation, Victoria, British Columbia

Bouzari, F., Lee, R.G., Hart, C.J.R. and van Straaten, B.I. (2021): Mineralogical and geochemical vectors within advanced argillic-altered rocks of north-central British Columbia (NTS 094E/02, 15, 104I/05); *in* Geoscience BC Summary of Activities 2020: Minerals, Geoscience BC, Report 2021-01, p. 91–104.

Introduction

Advanced argillic-alteration zones in the upper parts of porphyry copper systems, also known as 'lithocaps', have a blanket-like geometry with areal extents of >10 km^2, reach up to 1 km in thickness and form the largest near-surface footprints of porphyry copper systems. Indeed, two or more porphyry copper deposits may underlie some large, coalesced advanced argillic zones (Sillitoe, 2010), which may themselves host high-sulphidation epithermal-type gold deposits where they are preserved from erosion.

Zones of advanced argillic alteration are formed by an early stage of intense acid leaching of the wallrocks and a subsequent stage of weakly acidic fluid flow, which deposits sulphides and quartz (Simmons et al. 2005; Heinrich, 2007; Hedenquist and Taran, 2013). Advanced argillic-altered rocks contain various proportions of minerals such as sericite, andalusite, pyrophyllite, topaz, diaspore, corundum, zunyite, dickite, alunite, kaolinite, dumortierite and quartz (Meyer and Hemley, 1967). Similar to the deeper alteration in porphyry deposits, the advanced argillic-alteration zones are typically zoned. Minerals such as diaspore and andalusite with pyrophyllite occur at the roots of advanced argillic alteration above the porphyry system, whereas zones of residual quartz, quartz-alunite and quartz-kaolinite occur laterally in more permeable hostrocks at higher levels (Sillitoe, 1993, 2010; Hedenquist et al., 1998; Watanabe and Hedenquist, 2001).

The recognition of mineralogical and geochemical patterns within areas of advanced argillic alteration provides a fundamental opportunity to identify the presence of high-sulphidation epithermal gold and potential underlying porphyry mineralization. Advanced argillic-alteration zones in some porphyry deposits overprint earlier and deeper porphyry alteration, a phenomenon called 'telescoping' (Sillitoe, 2010) that results from the rapid collapse of the isotherms (Heinrich et al., 2004) or rapid uplift and erosion of the volcanic edifice (Sillitoe, 2010). Therefore, identification and characterization of advanced argillic alteration from pre-existing higher temperature alteration is important in establishing the vertical profile of the deposit and its potential hypogene enrichment at depth.

Advanced Argillic Alteration in BC

Advanced argillic alteration is not a common feature in many porphyry deposits in British Columbia (BC); this is attributed to the erosion that has destroyed and removed the shallow parts of porphyry systems in many districts. However, advanced argillic-alteration zones are preserved in some locations in BC, typically within districts that are also highly prospective to host porphyry-type copper mineralization. More particularly, zones of advanced argillic alteration cover large areas in northern BC and Vancouver Island. Studies in the Toodoggone district (Bouzari et al., 2019), the Bonanza volcanic field in northern Vancouver Island (Panteleyev and Koyanagi, 1994), Limonite Creek in central BC (Deyell et al., 2000) and several other locations in BC have recognized linkages of these altered zones to porphyry-type mineralization at depth.

Mineral exploration within advanced argillic zones is traditionally difficult because of the large size of the altered areas, the intense nature of the alteration and the subtle mineralogical changes that can be difficult to identify in the field or with tools such as a hand lens. Identification of the tex-

This publication is also available, free of charge, as colour digital files in Adobe Acrobat® PDF format from the Geoscience BC website: http://geosciencebc.com/updates/summary-of-activities/.

tural, mineralogical and geochemical trends within these advanced argillic-alteration zones will guide BC explorers to better identify porphyry copper potential and to provide tools that point toward associated mineralization.

In this study, alteration-mineral assemblages and compositions across advanced argillic-alteration zones in three BC mineral properties are characterized: the Tanzilla mineral property, near Dease Lake, and the Alunite Ridge and Kemess North mineral properties, both in the Toodoggone district (Figure 1). The mineralogical and geochemical data from these locations are used to establish tools and protocols that can be used to explore for porphyry deposits in areas with advanced argillic alteration anywhere in BC. This paper provides an update to the Geoscience BC-sponsored research project on advanced argillic alteration (Bouzari et al., 2020) and will be superseded by a final report to be published later in 2021.

Geological Setting

Advanced argillic-alteration zones occur in several locations in BC, particularly in porphyry-prospective areas of northern BC and Vancouver Island (Panteleyev and Koyanagi, 1994; Bouzari et al., 2020). Tanzilla, Alunite Ridge and Kemess North are located in the Stikine terrane of northern BC. The geological setting and mineral occurrences of these mineral properties have been described in several previous studies (e.g., Diakow, et al., 1993, 2006; van Straaten and Gibson 2017). The geological setting of these research sites has also been reviewed previously (Bouzari et al., 2020) and only brief summaries are provided here.

Tanzilla

The Tanzilla property is underlain by a volcanic succession assigned to the Horn Mountain Formation (late Early to

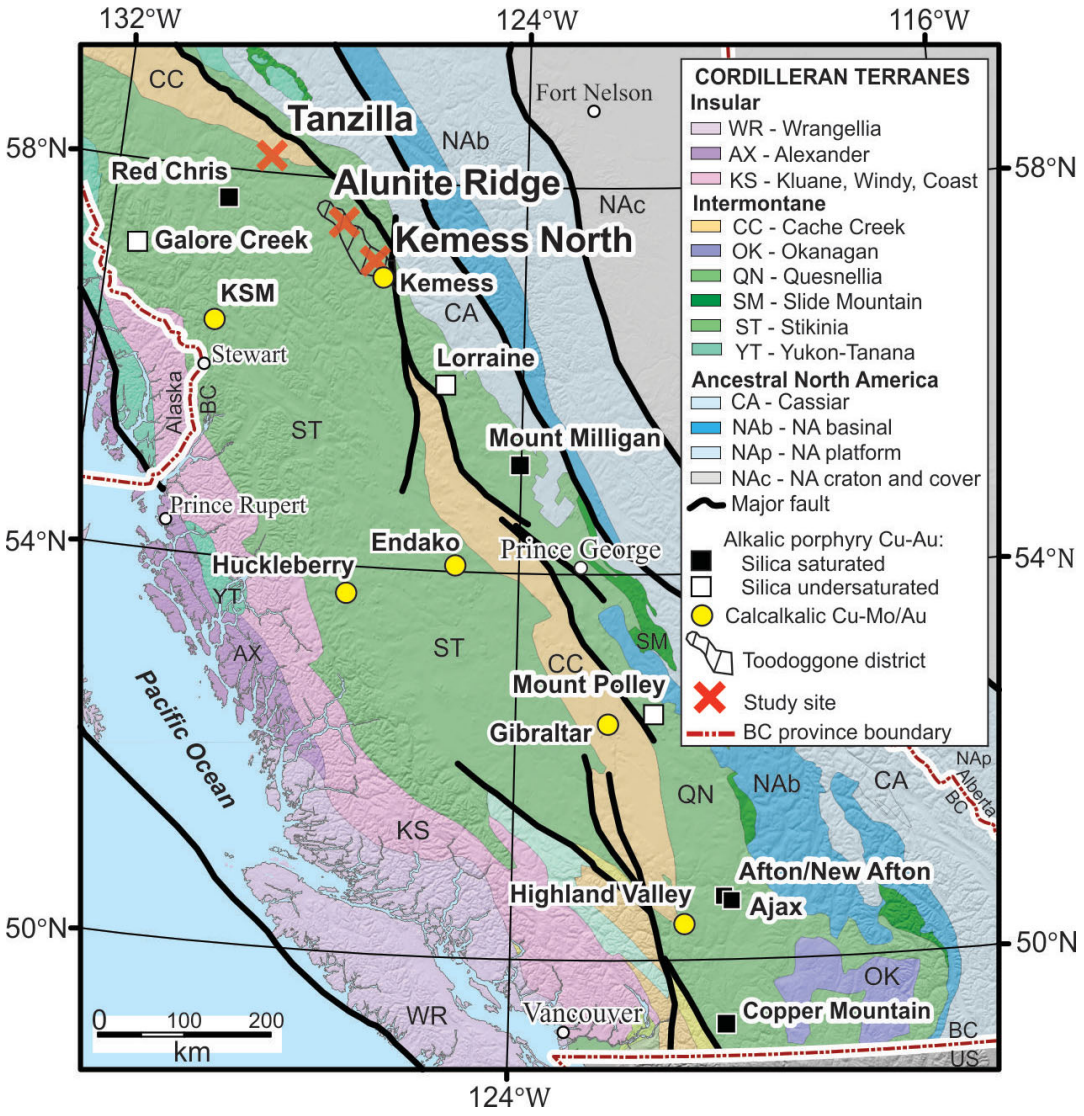

Figure 1. Cordilleran terranes of British Columbia showing the location of the study areas (after Bissig and Cooke, 2014).

Middle Jurassic; van Straaten and Nelson, 2016) in the upper part of the Hazelton Group (Figure 2). The lower part of the Horn Mountain Formation includes massive green augite-plagioclase–phyric volcanic breccia (not exposed in the study area), whereas the middle part is mainly maroon volcanic breccias, autobreccias and flows, and includes minor laminated felsic tuffs to bedded lapillistone. The upper parts of the Horn Mountain Formation consist of a felsic volcanic unit of mainly aphanitic and plagioclase-phyric clasts capped by a mafic volcanic unit of augite-plagioclase–phyric volcanic breccia and flows (van Straaten and Gibson, 2017). These units are unconformably overlain by sedimentary rocks of the Bowser Lake Group. The Late Jurassic Snowdrift Creek pluton cuts the Horn Mountain strata and the Kehlechoa thrust fault. The Horn Mountain Formation hosts areally extensive advanced argillic alteration at the Tanzilla-McBride property for at least 17 km along strike (van Straaten and Gibson, 2017; van Straaten and Bouzari, 2018). At Tanzilla, the advanced argillic-alteration zone is at least 5 by 2 km and overlies porphyry-style alteration at depth, which is characterized by quartz-sericite-pyrite to potassic alteration with anomalous copper and molybdenum hosted in a 173 Ma plagioclase porphyry intrusion (van Straaten and Nelson, 2016; van Straaten and Gibson, 2017).

Alunite Ridge

Alunite Ridge is located within the Toodoggone district of northeastern BC. The district hosts several preserved Early Jurassic high- and low-sulphidation epithermal-type deposits with advanced argillic-alteration zones (Diakow et al., 1993; Bouzari et al., 2019). The Alunite Ridge area near Quartz Lake hosts several mineral occurrences, including Quartz Lake, Alunite Ridge, North Ridge and Sickle Creek (Figure 3). The underlying geology consists of the Lower Toodoggone Formation, which is equivalent to the Telkwa Formation of the Hazelton Group (Diakow et al., 1991), and consists of andesitic lava flows, tuff, breccia and epiclastic rocks that are intruded by small dikes and stocks of monzonite (Figure 3). The Jock Creek monzonitic pluton forms a large body to the south and east. Zones of intense alteration are northwest-trending and about 200 m wide. Gold mineralization occurs in a 10–15 m wide zone of silicified rock with quartz-alunite alteration, locally with vuggy textures and zones of buff-grey intense diaspore alteration (Bouzari et al., 2019). Banded quartz veins with calcite and K-feldspar host low-sulphidation–type chalcopyrite-sphalerite-galena-pyrite mineralization and occur 200–300 m south of the advanced argillic-altered zone at Alunite Ridge and at the base of the valley near Quartz Lake.

Kemess North

The Kemess North porphyry is located about 6.5 km north of the main Kemess deposit (Kemess South) in the southern part of the Toodoggone district. Hostrocks at Kemess North include Upper Triassic Takla Group andesite/basaltic volcanic rocks locally overlain by Lower Jurassic Toodoggone Formation dacitic fragmental volcanic rocks (Figure 4). Several Early Jurassic stocks or dikes of quartz monzonite to quartz rhyolite composition of the Black Lake intrusive suite have intruded the volcanic succession (McKinley,

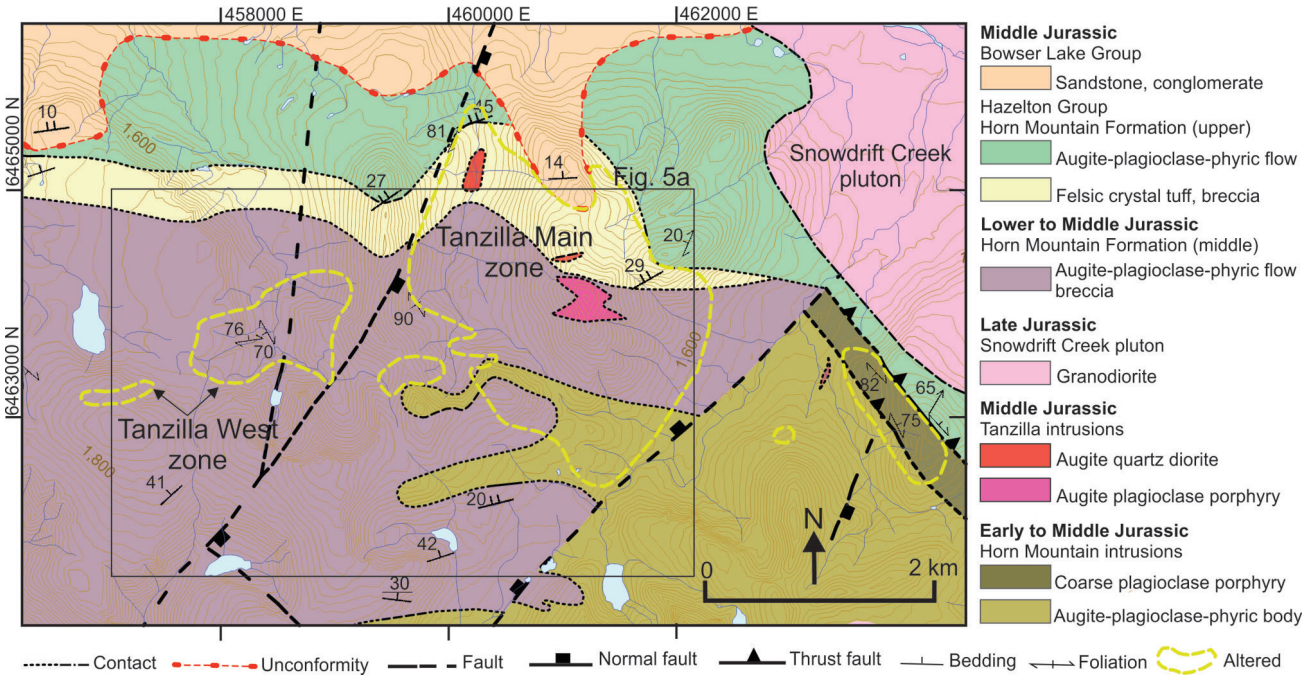

Figure 2. Geology of the Tanzilla study area (after van Straaten et al., 2017).

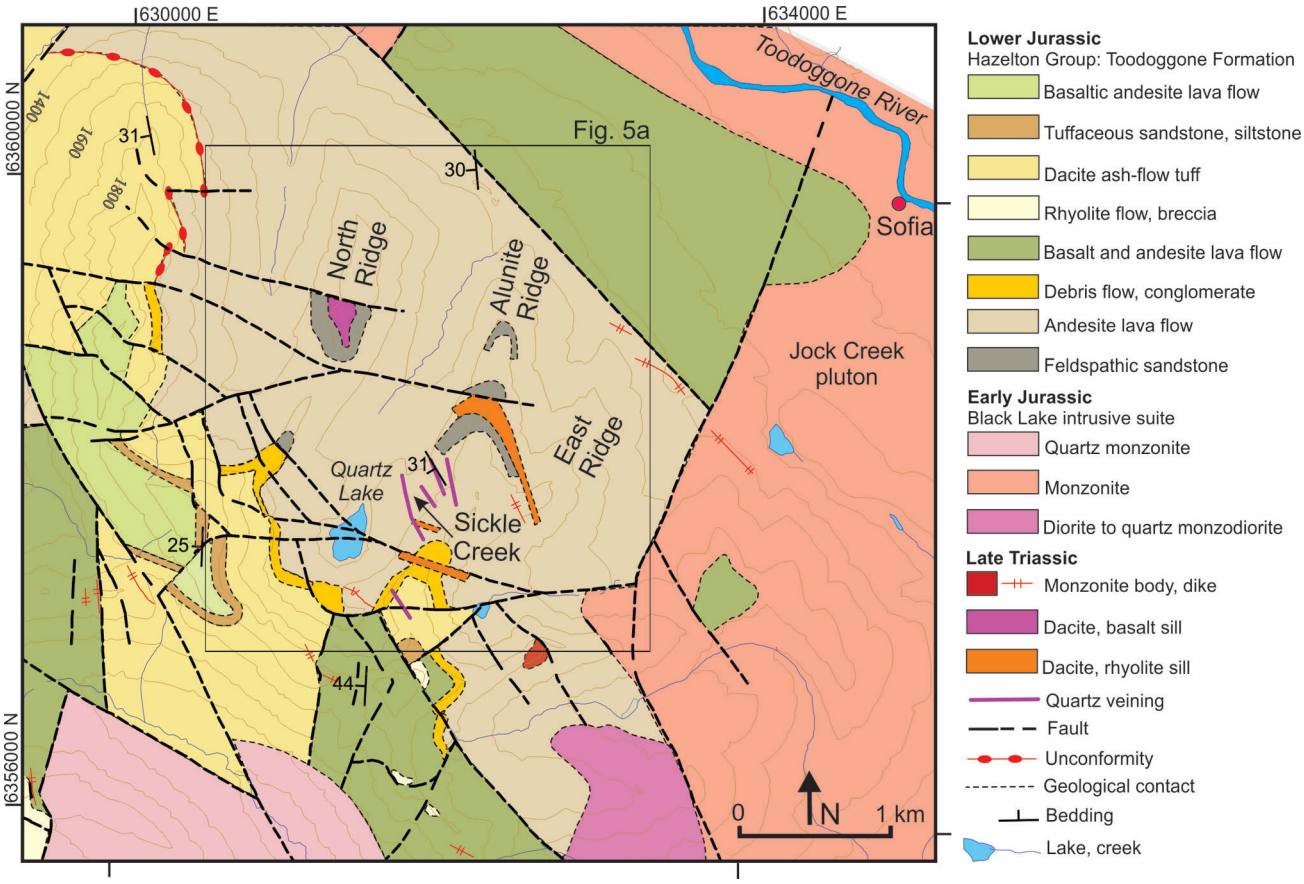

Figure 3. Geology of the Alunite Ridge study area (after Diakow et al., 2006).

2006). The east-trending, south-dipping mineralization at Kemess North seems to have formed along faults with distinct sericite-clay alteration near the surface, which transitions to typical K-silicate alteration at depth.

Sampling and Analytical Work

At Tanzilla, advanced argillic alteration was mapped and sampled across a 3.5 km north–south profile and a 4 km east–west profile. A total of 54 samples were collected from surface outcrops. Drillhole TZ15-01 (Barresi and Luckman, 2016), which tested mineralization below the Main zone hill to the depth of 840 m (-60°) was examined, and 20 core samples were collected to characterize alteration and mineralization at depth. At Alunite Ridge, the footprint of alteration was mapped and sampled along three northeast-trending profiles with a total length of approximately 5 km in an area of 2 by 2 km. In total, 63 samples from surface outcrops ranging in elevation from 1908 to 1560 m asl and 10 samples from drillhole SG-04-18 (Kuran and Barrios, 2005) to a depth of 227 m below surface (1642 m asl) were collected. At Kemess North, advanced argillic alteration was mapped and sampled along a north–south profile of approximately 0.5 km. In total, 18 samples were collected from surface outcrops. Drillholes KN-01-12 and KN-02-09 (SRK Consulting Inc., 2016), which tested mineralization below the advanced argillic alteration to a depth of ~500 m below surface, were examined and 44 core samples were collected to characterize alteration and mineralization at depth. Surface sample locations are shown on Figure 5a and results for drillhole samples will be provided in a subsequent publication.

All rock samples were characterized in the field, and again after being cut into slabs. To further characterize alteration assemblages, all samples were analyzed at The University of British Columbia's Mineral Deposit Research Unit (MDRU) using the tabletop version of the Terraspec® by Analytical Spectral Devices (ASD) Inc., with full range visible and near-infrared (VNIR) and shortwave infrared (SWIR) wavelengths for the range of 350–2500 nm. Petrographic thin-section studies were completed for 56 selected rock samples. A total of 223 whole-rock samples were analyzed for major- and trace- elements at Bureau Veritas Minerals (Vancouver, BC). Samples were analyzed by X-ray fluorescence (XF700 method) for SiO_2, Al_2O_3, Fe_2O_3, CaO, MgO, Na_2O, K_2O, MnO, TiO_2, P_2O_5, Cr_2O_3, SO_3 and Sr; inductively coupled plasma (ICP)–mass spectrometry using lithium borate fusion (LF100) for Ba, Be, Co, Cs, Ga, Hf, Nb, Rb, Sn, Sr, Ta, Th, U, V, W, Zr, Y, La, Ce, Pr, Nd, Sm, Eu, Gd, Tb, Dy, Ho, Er, Tm, Yb and Lu; multi-acid digestion followed by ICP–emission spectrome-

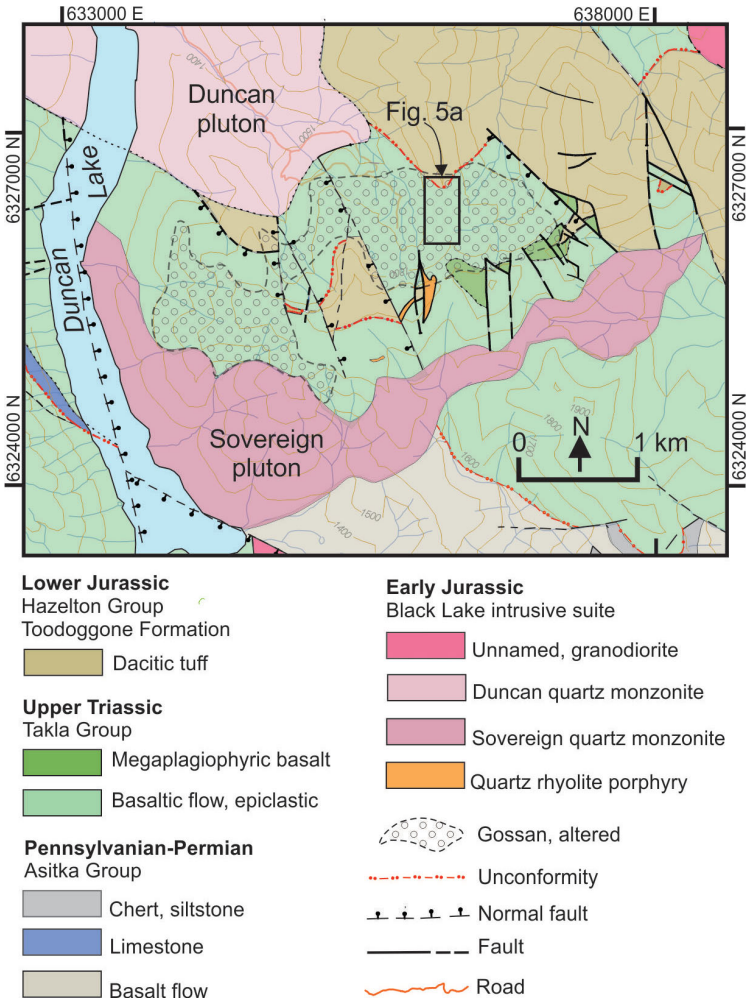

Figure 4. Geology of the Kemess North study area (after Diakow, 2001), showing location of area sampled (Figure 5a).

try and ICP–mass spectrometry (MA200) for Mo, Cu, Pb, Zn, Ag, Ni, As, Cd, Sb, Bi, Sc, Se and Tl; and Au by fire assay/atomic absorption spectroscopy. In addition, magnetic susceptibility of all collected rocks was measured with a KT-10 magnetic susceptibility meter manufactured by Terraplus Inc. Rock density and porosity of all collected rocks were measured using saturation and buoyancy techniques at MDRU (Ulusay and Hudson, 2007). Results of the physical properties of the rock samples will be provided in the final report.

Alteration Mineralogy

Tanzilla

Tanzilla includes two alteration zones: the Main zone (>4 km^2) and the West zone (Figure 2). Field and SWIR data (Bouzari et al., 2020) show that alteration at Tanzilla is characterized by a green sericite-chlorite–assemblage (Figures 6e, 7a) zone that grades, toward the zones of advanced argillic alteration at the hill in the Tanzilla Main zone, to a pale green sericite and then to a white sericite assemblage (Figures 6c, 7c) with pyrophyllite and topaz (Figure 5b). In more central locations and commonly at higher elevations, the alteration is characterized by highly silicified rock with remnant sericite, pyrite, and locally abundant pyrophyllite and topaz (Figures 6a, 7d). The sericite at the Main zone is typically muscovite and strongly crystalline (Bouzari et al., 2020). Alteration outside of the green sericite-chlorite assemblage zone is dominantly darker green chlorite-sericite (Figure 6f) and more distal patchy chlorite-epidote alteration occurs within the volcanic rocks (Figure 5b). The chlorite alteration is pervasive and locally alters an earlier biotite alteration.

Alunite Ridge

Advanced argillic alteration in the Alunite Ridge area occurs for over 2 km along a north-northeast-trending ridge (Alunite Ridge) and extends further to the north along North Ridge and to the east along East Ridge (Figures 3, 5b). Field observations backed by SWIR data indicate that the central part of the Alunite Ridge property is characterized by an alteration zone of strong silicification

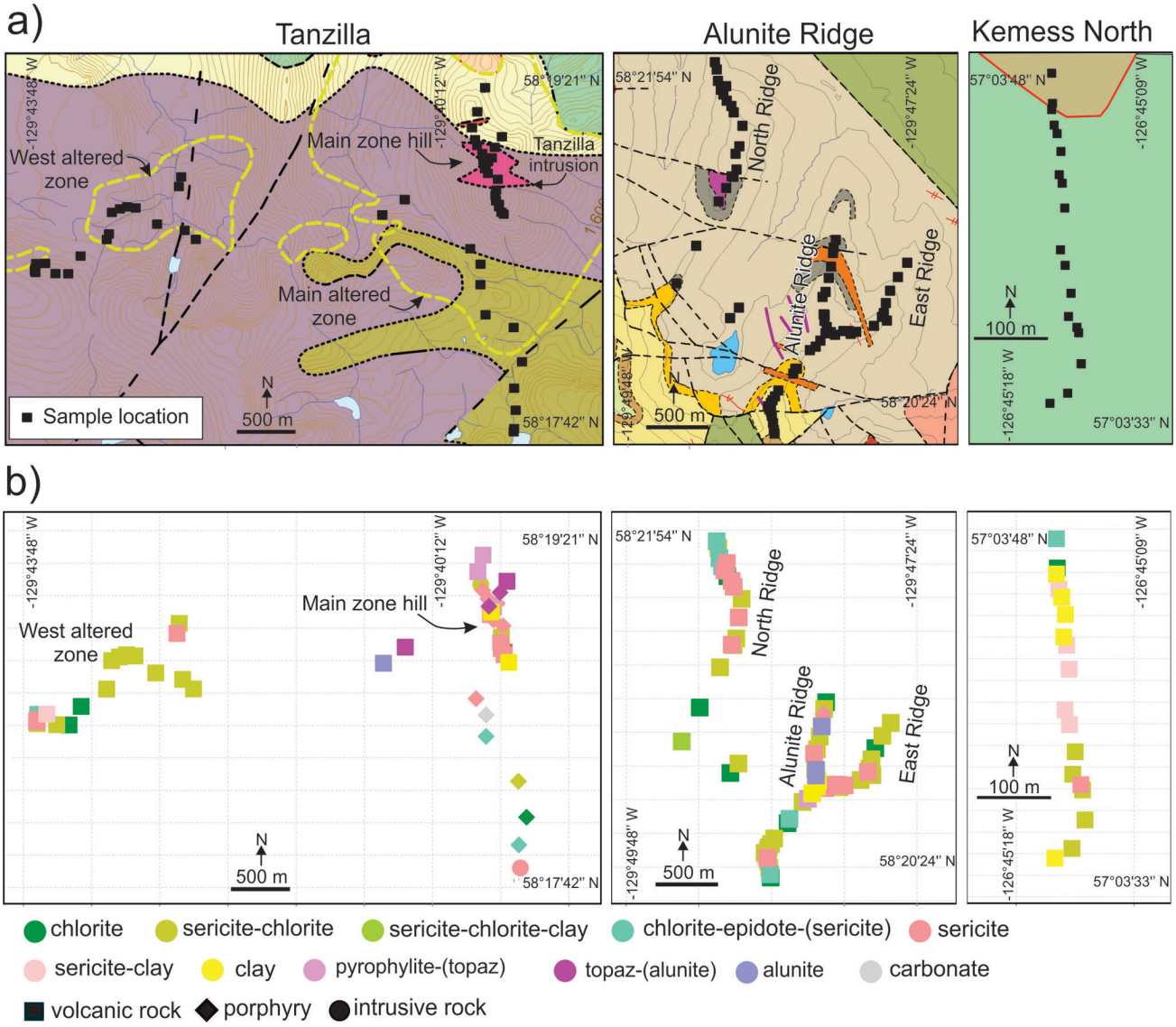

Figure 5. Location of samples from the Tanzilla, Alunite Ridge and Kemess North study areas: **a)** distribution relative to the regional geology (see Figures 2–4 for legend of geological units); **b)** distribution of alteration-mineral assemblages identified by shortwave-infrared analyses.

with alunite, kaolinite, dickite, sericite and locally pyrophyllite. The sericite is typically poorly crystalline illite (Bouzari et al., 2020). This zone is surrounded by an alteration zone of pale green pervasive sericite with weakly altered to intermediate, fine- to medium-grained chlorite and pyrite, which is generally disseminated but also occurs in thin veinlets largely oxidized to jarosite and hematite (Figures 6d, 7b). This alteration gradually transitions to the north and east to darker green alteration of chlorite-sericite and locally epidote occurs more distally (Figure 5b).

Kemess North

The alteration zone exposed at the surface at the north-trending Kemess North ridge is hosted by basaltic flows of the Takla Group and is distinctly zoned from south to north (Figures 4, 5b). In the southern parts of the ridge, alteration is characterized by green sericite-chlorite and gradually transitions northward to a green-grey sericite (illite) assemblage and then to grey-white sericite-dickite-kaolinite typically with pervasive silicification and quartz veins (Figure 5b). Clay alteration of kaolinite and dickite forms along fractures, and vugs fill with sericite associated with the silicification (Figure 6b). The silicification can reach as much as 30 vol. %, with clay alteration making up the remaining volume. This strongly argillic-altered Takla rock is in fault contact with the chlorite-epidote–altered volcanic rocks of the Toodoggone Formation to the north. Illite crystallinity increases northward (Bouzari et al., 2020). Pyrite is abundant (>2%), occurring as disseminations and stockwork of quartz veins.

Hostrock Composition

Hostrock composition affects the type and intensity of alteration assemblages. Therefore, it is important to characterize hostrocks and their influence on alteration to identify alteration-related vectors. Data from available geological maps as well as field observations have been used to classify rock types. Geochemical trace-element data can also be used to characterize the hostrocks following methods described by Halley (2020). A V versus Sc scatterplot has been used to distinguish volcanic rocks of the Takla Group from those of the Hazelton Group (Figure 8a). Both V^{3+} and Sc^{3+} have similar behaviour and substitute for Fe in amphibole, pyroxene and biotite during crystallization (Li and Lee, 2004; Halley, 2020). All hostrocks show a positive trend of Sc against V (Figure 8a); however, the slope of the trend is slightly different, with the Takla Group showing the least amount of change with increasing V compared to the Toodoggone Formation rocks, which display the highest degree of change. The Horn Mountain Formation rocks plot between the other two units.

A Th versus Sc scatterplot is useful to characterize mafic to felsic composition of the hostrocks. The Th versus Sc diagram (Figure 8b) shows that all rock units have similar Sc, except some Takla samples that display the highest Sc values; higher Sc means lower Si in the rock. There is a weak negative correlation between Sc and Th values, especially for Takla Group and Toodoggone Formation rocks. However, the Th content shows some distinct variations: Takla Group volcanic rocks, relative to Hazelton Group rocks (Toodoggone and Horn Mountain formations), have lower Th concentrations; within the Hazelton Group, the Horn Mountain Formation has the largest degree of scatter relative to high Th values. The Sc concentration corresponds to high-Fe rocks and Th, an incompatible element, stays in the melts and incorporates into late-stage crystalizing mineral phases (Pearce and Norry, 1979). Therefore, the trend from high Sc to high Th reflects a change in composition from more mafic Takla volcanic rocks to mafic-intermediate felsic rocks of the Toodoggone and Horn Mountain formations. A similar diagram of Th versus Sc colour-coded by alteration assemblage (Figure 8c) shows that there is no distinct hostrock influence and that the fluids dictate the distribution of alteration assemblages. Although rocks with higher Th (>~8 ppm) do not show signs of chlorite-dominated alteration, they still show biotite and sericite-chlorite alteration. Therefore, it is possible that more felsic rocks of the Hazelton Group have developed weaker chlorite-type alteration, but the available data suggest that this was not

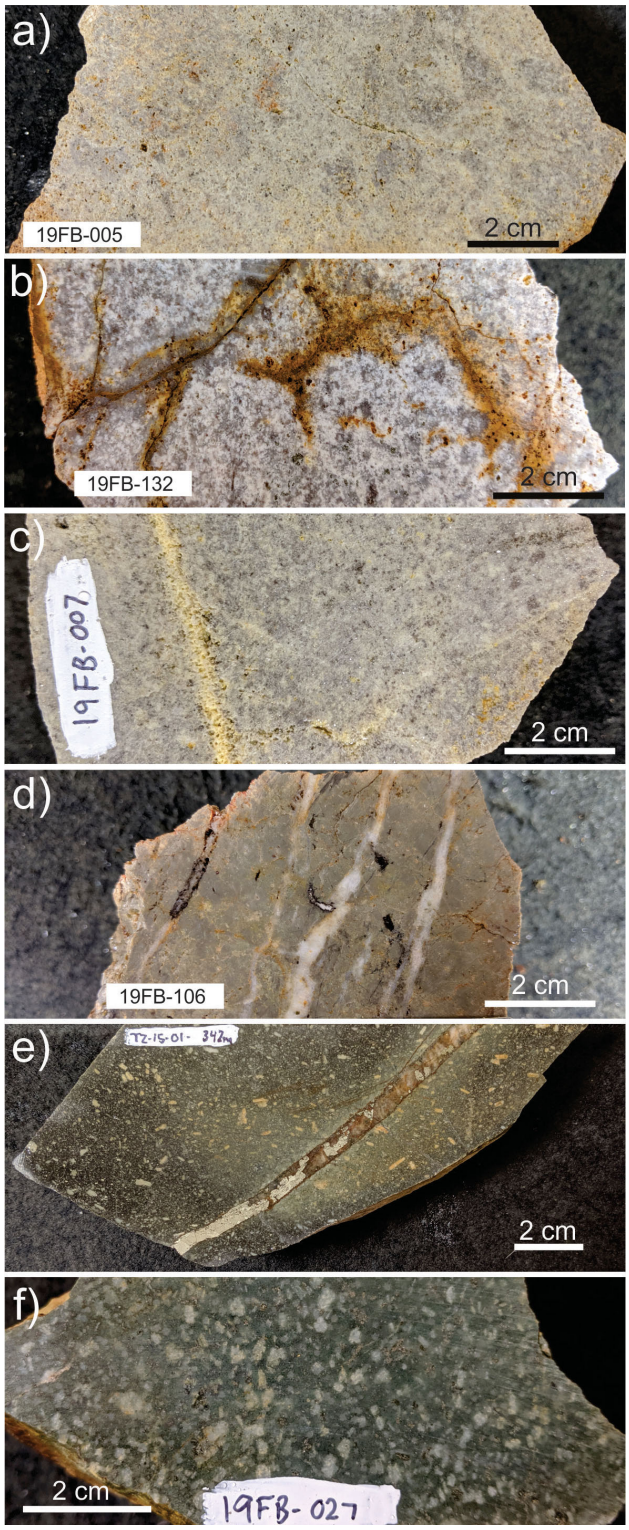

Figure 6. Representative rock samples of alteration assemblages from the study areas: **a**) plagioclase-phyric volcanic rock from Tanzilla with pervasive silicification, minor vuggy texture and pale yellow to grey alteration of pyrophyllite and topaz; **b**) Takla Group volcanic rock from Kemess North with strong kaolinite-dickite alteration and silicification; **c**) plagioclase-phyric volcanic rock(?) from Tanzilla with pervasive white sericite (muscovite) alteration; **d**) Toodoggone Formation volcanic rock from Alunite Ridge with pervasive pale green sericite alteration and silicification cut by quartz veinlets; **e**) plagioclase porphyry from Tanzilla with green sericite-chlorite alteration and remnants of fine-grained disseminated biotite cut by a quartz-pyrite vein; **f)** plagioclase porphyry from the margin of the advanced argillic-alteration zone at Tanzilla, with strong pervasive chlorite-sericite alteration.

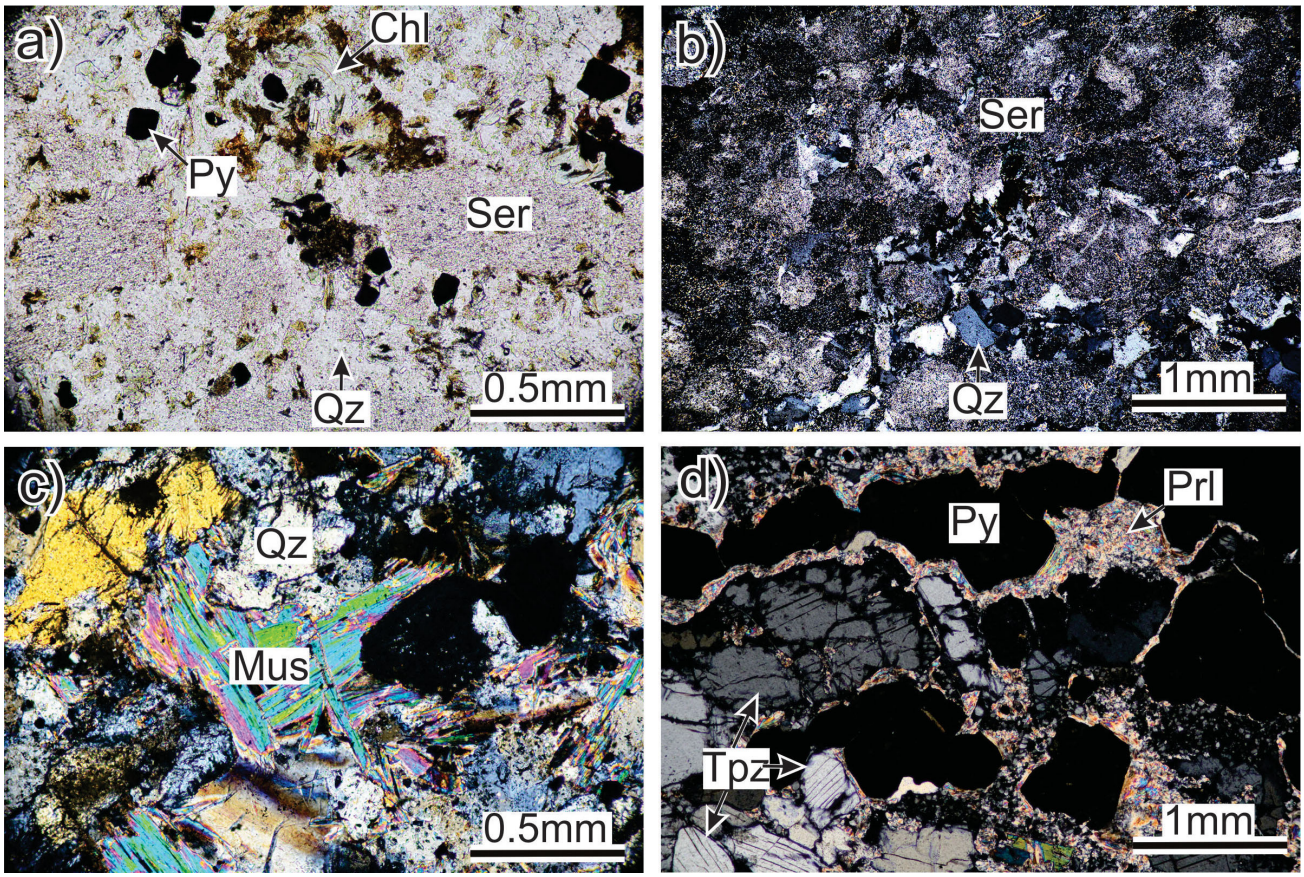

Figure 7. Photomicrographs of selected alteration assemblages from the study areas: **a**) pervasive texturally destructive green sericite-chlorite alteration of groundmass showing chlorite after mafic phases, with remnants of feldspar grains altered to fine-grained sericite (sample from Tanzilla intrusive rock); **b)** pale green sericite alteration showing pervasive fine-grained sericite with quartz, hosted in volcanic rock from Alunite Ridge, and with remnant sulphide and magnetite still present as opaque phases; **c)** white sericite alteration showing coarse muscovite with quartz, hosted in volcanic rock (sample from Tanzilla volcanic breccia) ;**d)**. veinlet-controlled topaz and pyrophyllite alteration with pyrite (sample of felsic crystal tuff from Tanzilla). Mineral abbreviations: Chl, chlorite; Ms, muscovite; Prl, pyrophyllite; Py, pyrite; Qz, quartz; Ser, sericite; Tpz, topaz.

significant and alteration types are scattered throughout various rock units.

A V/Sc versus Sc diagram is also used to discriminate between rock types (Halley, 2020) and to determine this factor's possible influence on alteration intensity. A slight decrease in V/Sc ratios in all rock units is associated with a lower Sc content (Figure 8d), corresponding to higher SiO_2. This decrease is attributed to the crystallization of magnetite, which incorporates V (Halley, 2020). A similar diagram, but colour-coded by intensity of alteration (Figure 8e), shows that hostrocks exercise no distinct control on intensity of alteration (e.g., alteration intensities from weak to very strong occur in all rock units). However, there is an increase in the V/Sc ratio at lower Sc concentration. A high V/Sc ratio has been used to indicate early crystallization of hornblende and clinopyroxene in fertile hydrous magmas (Loucks, 2014). Given the limited number of samples, it is difficult to argue that some of the hostrocks in the study area had originated from more fertile magmas. Comparing the values from Figure 8d with those representing the intensity of alteration (Figure 8e), it appears that in this dataset, the high V/Sc values may have been caused by intense advanced argillic alteration, especially intense silicification. Therefore, it is possible that strong alteration in advanced argillic-altered rocks can increase the V/Sc ratio of the rock.

Geochemical Vectors

Trace-element geochemical data can be used in the advanced argillic-alteration environment to provide vectoring guidance that can assist in indicating proximity to porphyry copper mineralization. Copper is not present in notable concentrations in advanced argillic-altered rocks of the study areas. In fact, Cu seems to have been depleted (<100 ppm) within the zones of strong advanced argillic alteration relative to the rocks associated with distal sericite-chlorite alteration (Figures 5b, 9a). The supergene oxidation may have further contributed to the low copper concentration at near surface. Gold locally shows weak anomalies (~0.1 ppm) in advanced argillic-altered rocks at

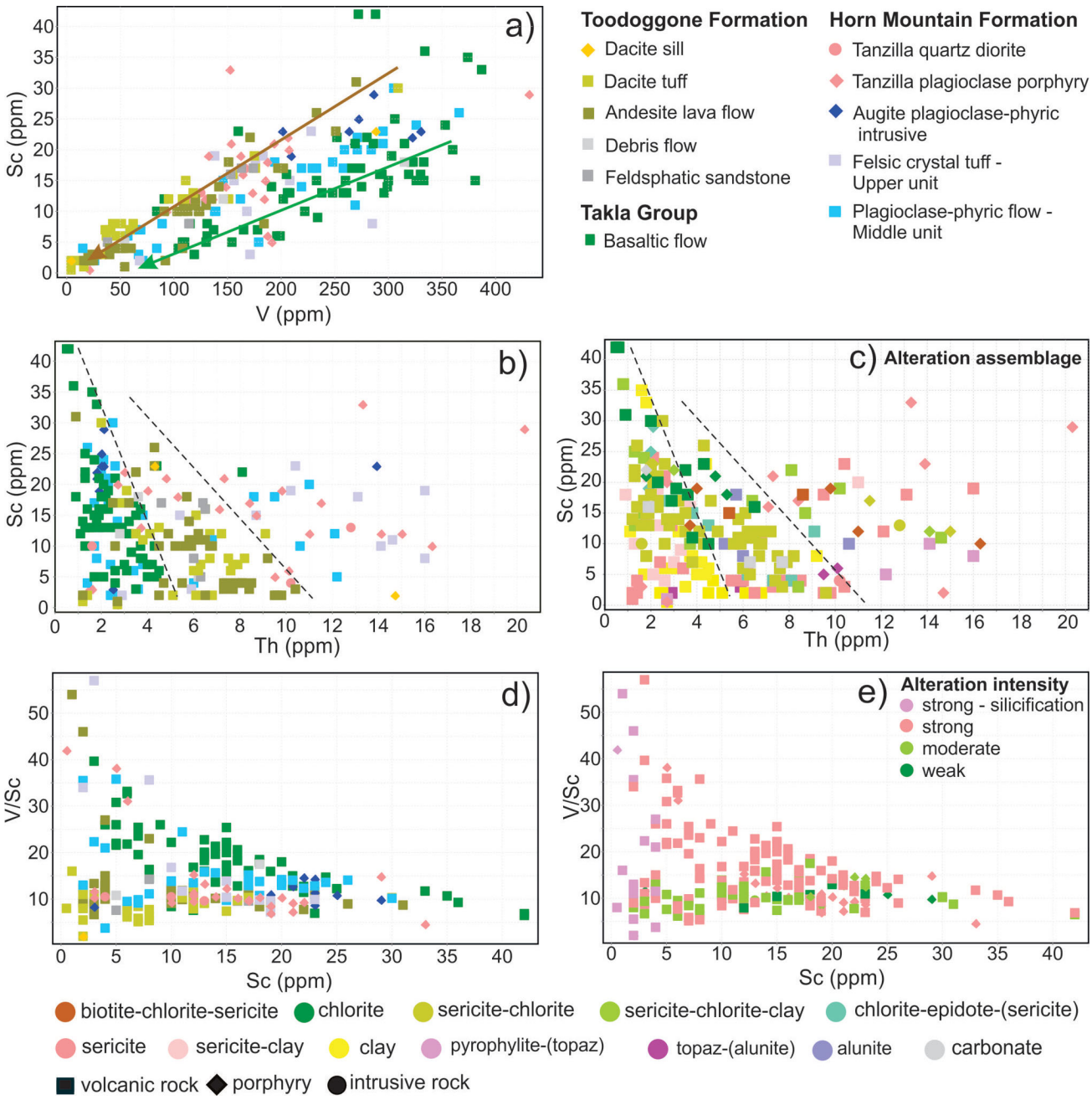

Figure 8. a) Scatterplots used to distinguish rocks of the Takla Group from those of the Hazelton Group in the study areas: **a)** V versus Sc diagram showing hostrock composition (arrowed lines show the main compositional trends); **b)** Th versus Sc scatterplot showing hostrock composition (dashed lines separate the main compositional changes); **c)** same diagram as in (b) but colour-coded by alteration assemblages; **d)** V/Sc versus Sc scatterplot showing hostrock composition; **e)** same diagram as in (d) but colour-coded by alteration intensity.

Tanzilla and Alunite Ridge, but the data do not reveal a clear trend. At Kemess North, there are higher concentrations of Au occurring within the sericite-chlorite–altered rocks in the southern parts of the ridge, whereas Au values are < 0.1 ppm in the sericite-clay–altered rocks on the northern side of the ridge (Figure 9b). Anomalous As concentrations occur with the advanced argillic alteration at Alunite Ridge (23 to 236 ppm) and Tanzilla (14 to 23 ppm), whereas the As concentration at Kemess North is low (<2 ppm; Figure 9c). This suggests a deeper setting for the alteration at Kemess North relative to Tanzilla and Alunite Ridge, as predicted from the alteration mineralogy (Bouzari et al., 2020). Zinc is largely depleted from the zone of advanced argillic alteration at Tanzilla and from the zone of intense sericite-clay alteration at Kemess North (<30 ppm). At Alunite Ridge, zinc distribution is variable within the

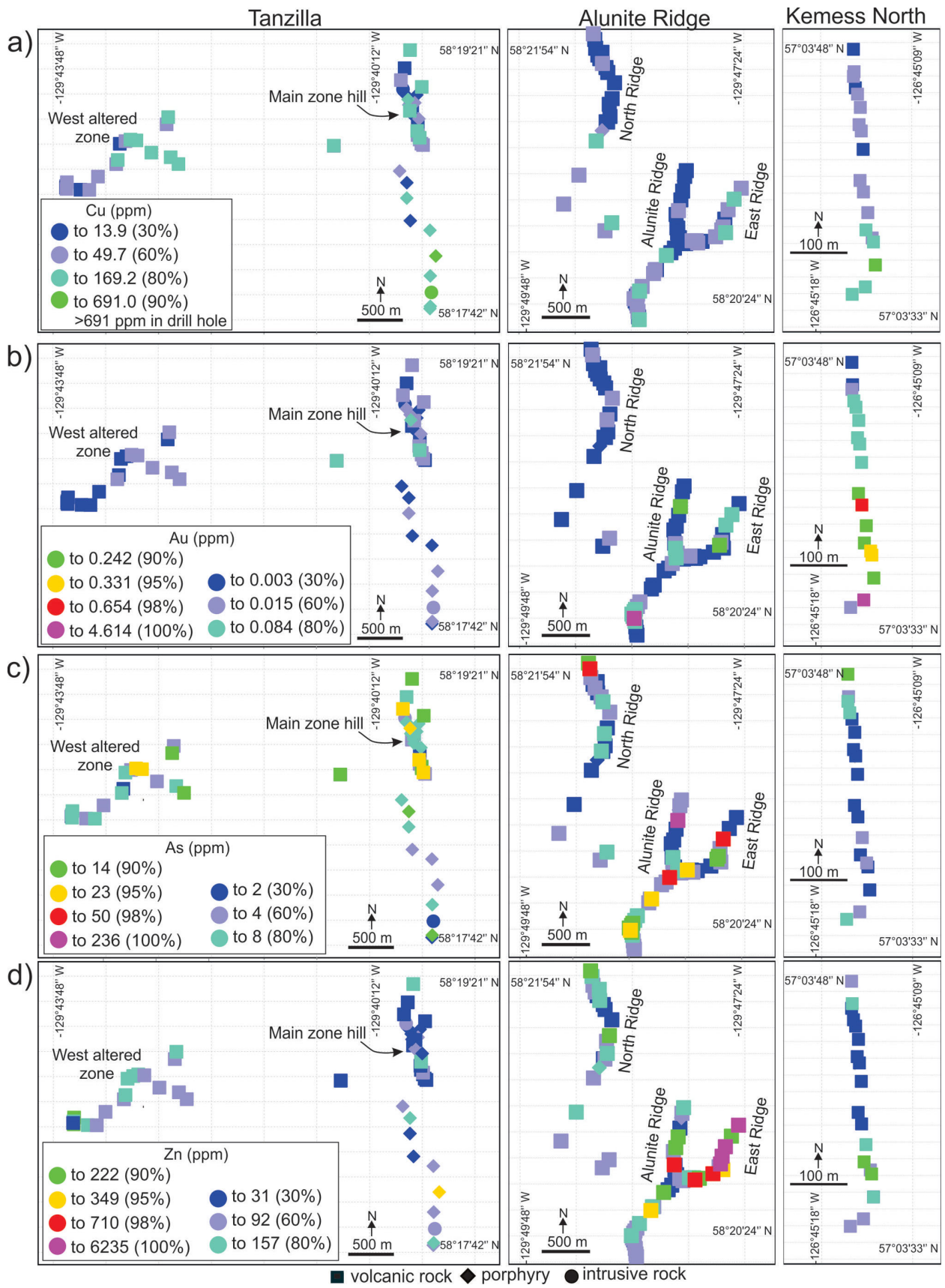

Figure 9. Trace-element distribution in the Tanzilla, Alunite Ridge and Kemess North mineral properties, showing **a)** Cu, **b)** Au, **c)** As, and **d)** Zn.

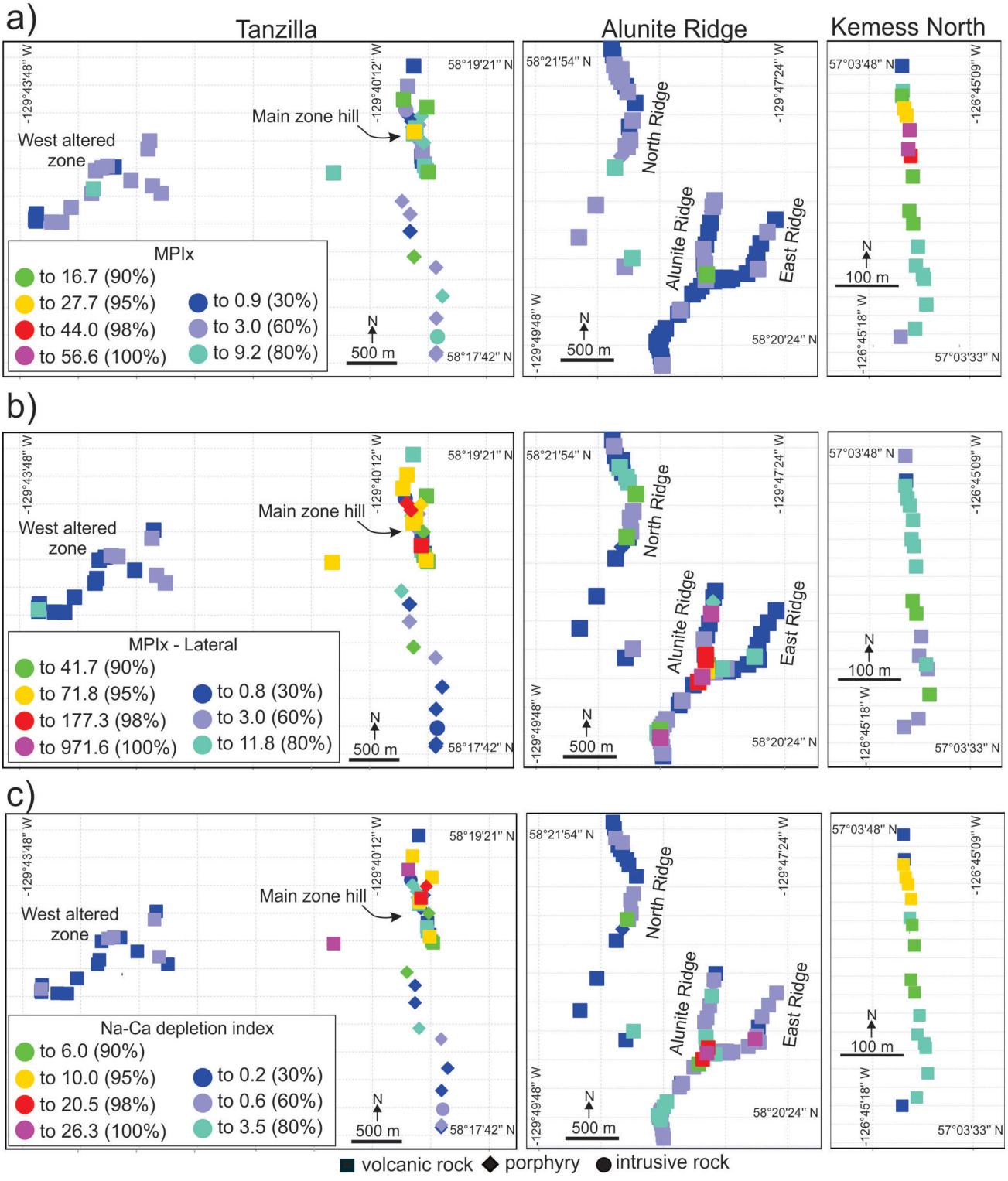

Figure 10. Distribution of relative proportion of elements (samples colour-coded) occurring at various levels of porphyry deposits at the Tanzilla, Alunite Ridge and Kemess North study areas determined using **a)** the MDRU Porphyry Index (MPIx), **b)** the MDRU Porphyry Index-Lateral (MPIx-Lateral), and **c)** the Na-Ca depletion index.

East Ridge, distal to the main area of Alunite Ridge, which shows the highest concentration (>700 ppm; Figure 9d).

MPIx

Whereas the concentration of metals can provide evidence for mineralization, its applicability to vectoring is affected by the intensity of mineralization. Therefore, a ratio of the sum of selected elements provides a more robust vectoring indicator for mineralization. The MDRU Porphyry Index (MPIx; Bouzari et al., 2019) compares the relative proportion of elements occurring at deeper levels of porphyry deposits (Cu, Mo, Sn, W) to those occurring at shallower levels (Sb, As, Ag, Tl, Li). Application of this index to the current study (Figure 10a) shows that, on a vertical profile, Kemess North has the highest MPIx and therefore represents a deeper level of alteration relative to Tanzilla, or to Alunite Ridge that shows the shallowest geochemical signature. The MPIx ratios vector toward the zones of intense central alteration, especially toward the northern side of the ridge at Kemess North and toward the hill in the Tanzilla Main zone. At Alunite Ridge, the MPIx shows the main central parts of the alteration but the vectoring signature is weak and dominated by very low MPIx values.

MPIx-Lateral

The MPIx provides a powerful tool to map the vertical proximity and vector to porphyry copper mineralization. However, at very shallow levels of porphyry copper systems, especially within areas of strong advanced argillic alteration, elements such as Cu, Mo, W and Sn are typically at very low concentrations over much of the altered area and the resulting MPIx value may not provide a lateral vector toward the top-central parts of the porphyry system. To complement the MPIx, the MDRU Porphyry Index-Lateral (MPIx-Lateral) is introduced, which compares metals that are enriched in the shallow parts of a porphyry system (Sb, As, Tl) to those that are more laterally dispersed (Halley et al., 2015) and typically have higher concentrations in more distal parts of the porphyry system (Zn, Mn). Element concentrations are multiplied or divided by an appropriate factor for normalization:

$$\text{MPIx-Lateral} = \frac{(5 \times Sb) + (20 \times Tl) + As}{\frac{Zn}{10} + \frac{Mn}{50}}$$

The MPIx-Lateral (Figure 10b) maps the advanced argillic alteration at the hill in the Tanzilla Main zone, where its footprint shows gradually decreasing values to the east and south. It also shows the Alunite Ridge central zone with decreasing values toward North Ridge. At Kemess North, the MPIx-Lateral values are weaker relative to Tanzilla and Alunite Ridge but still vector toward the more intensely altered parts of the ridge.

Na-Ca Depletion Index

Zones of advanced argillic alteration are characterized by intense removal of many rock-forming elements, particularly Ca and alkali metals such as K and Na, due to leaching of the hostrock by low-pH fluids. Therefore, zones of advanced argillic alteration and areas with the highest intensity of alteration will be characterized by elemental loss. Potassium is usually fixed with the formation of pervasive sericite alteration but Ca and Na depletion, in most cases, correlates with the intensity of advanced argillic alteration. The following elemental ratio is suggested to map the Na-Ca depletion using the sum of the rare-earth elements (REE) as an immobile factor (all values in ppm):

$$\text{Na-Ca depletion index} = \frac{\sum \text{REE}}{\text{Ca} + \text{Na}} \times 100$$

The application of the Na-Ca depletion index to the study sites shows that the zones of most intense advanced argillic alteration have the highest level of Na and Ca depletion, with the index gradually decreasing distally (Figure 10c). At Kemess North, where sericite-clay alteration is dominant, the Na and Ca depletion is less intense compared to the advanced argillic alterations at Tanzilla and Alunite Ridge but still vectors, with increasing Na-Ca depletion northward, toward the zone of more intense clay alteration.

Conclusions

Mineralogical and geochemical data and information can all be used individually or integrated to characterize the advanced argillic-alteration environment and to provide tools that identify zoning within the study sites. Variations in alteration assemblages and geochemical signatures suggest that the study sites represent different levels of advanced argillic or shallow-level alteration potentially above a porphyry copper system. Alunite Ridge represents the shallowest levels among the study sites, with abundant silicification, alunite, arsenic, local pyrophyllite and low MPIx ratios. Tanzilla represents slightly deeper levels, with abundant pyrophyllite and topaz alterations, moderate As concentrations and moderate MPIx ratios. Kemess North probably represents a relatively deeper environment, with abundant sericite and dickite alterations and the highest MPIx ratios. High-level lateral zoning is characterized in this paper, in which the following characteristics have been shown to be useful as vectoring tools to identify trends toward the central parts of advanced argillic-alteration zones and potentially the region above the underlying porphyry copper mineralization:

1) Regions of advanced argillic alteration are mineralogically zoned. The central parts of the advanced argillic-alteration zone typically contain variable zones of strong silicification. Topaz, andalusite, alunite and pyrophyllite occur within the silicified rocks and vari-

able types of sericite typically occupy the central and most intensely altered parts of advanced argillic-alteration zones. These are zoned outward (distally) to sericite and clay (kaolinite-dickite) mineral assemblages, forming white to grey sericite-(clay) alteration. This alteration is surrounded by a zone of pale green sericite alteration, which transitions outward to zones of green sericite-chlorite alteration. The SWIR data have shown that the sericite composition varies from K-rich to phengitic (Bouzari et al., 2020). More distally, the proportion of the chlorite increases and chlorite-epidote-(sericite) occurs near the least altered rocks.

2) A Na-Ca depletion index was developed to map Ca and alkali depletion within and around zones of advanced argillic alteration. Mapping of various intensities of Na-Ca depletion provides a vector toward zones of high fluid flow and potentially to the more central parts of alteration above a porphyry centre.
3) A new tool, the MDRU Porphyry Index-Lateral (MPIx-Lateral) was developed to map the geochemical vectors on a horizontal profile of shallow-level porphyry alteration. This index uses elements that are dispersed distally at shallow levels of porphyry deposits (Zn, Mn) relative to those occurring above a porphyry deposit (Sb, As, Tl) and, therefore, provides a complement to the MPIx as well as being useful for vectoring in the horizontal shallow-level space.

Further characterization of alteration mineralogy, quartz types and chemistry, determination of mineral abundance and mass gain/loss as well as work on the physical properties of the rock samples and mineral chemistry are underway, all of which will contribute to improving the toolbox used in the exploration of advanced argillic-alteration zones in BC.

Acknowledgments

Geoscience BC is thanked for its financial contribution in support of this project. Kaizen Discovery Inc. gave permission to visit the Tanzilla property and sample drillcore. Centerra Gold provided access to Kemess North and drillcore, as well as accommodation at the Kemess mine. The authors thank R. Billingsley for giving them the permission to visit the Alunite Ridge property. Field assistance was provided by Z. Boileau and B. Najafian helped with laboratory work. The authors thank H. Leal-Mejía, of the MDRU-Mineral Deposit Research Unit at The University of British Columbia, and staff members of Geoscience BC for their review of and comments on this paper.

References

Barresi, T. and Luckman, N. (2016): Diamond drilling report on the Tanzilla property, northwestern British Columbia; BC Ministry of Energy, Mines and Low Carbon Innovation, Assessment Report 36431, 46 p., URL <https://aris.empr.gov.bc.ca/ARISReports/36431.PDF> [September 2020]

Bissig, T. and Cooke, D.R. (2014): Introduction to the special issue devoted to alkalic porphyry Cu-Au and epithermal Au deposits; Economic Geology, v. 109, p. 819–825.

Bouzari, F., Bissig, T., Hart, C.J.R. and Leal- Mejía, H. (2019): An exploration framework for porphyry to epithermal transitions in the Toodoggone mineral district (94E); Geoscience BC Report 2019-08, MDRU Publication 424, 101 p., URL <http://www.geosciencebc.com/wp-content/uploads/2019/11/Geoscience-BC-Report-2019-08.pdf> [September 2020].

Bouzari, F., Lee, R.G., Hart, C.J.R. and van Straaten, B.I. (2020): Porphyry vectoring within advanced argillic-altered rocks of British Columbia; *in* Geoscience BC Summary of Activities 2019: Minerals, Geoscience BC, Report 2020-01, p. 115–130, URL <http://www.geosciencebc.com/i/pdf/SummaryofActivities2019/Minerals/Project%202018-022_Minerals_SOA2019.pdf> [September 2020].

Deyell, C.L., Thompson, J.F.H., Friedman, R.M. and Groat, L.A. (2000): Age and origin of advanced argillic alteration zones and related exotic limonite deposits in the Limonite Creek area, central British Columbia; Canadian Journal of Earth Sciences, v. 37, p. 1093–1107.

Diakow, L.J. (2001): Geology of the southern Toodoggone River and northern McConnell Creek map areas, north-central British Columbia (parts of NTS 94E/2, 94D/15 and 94D16); BC Ministry of Energy, Mines and Low Carbon Innovation, BC Geological Survey, Geoscience Map 2001-1, scale 1:50 000, URL <http://cmscontent.nrs.gov.bc.ca/geoscience/PublicationCatalogue/GeoscienceMap/BCGS_GM2001-01.pdf> [September 2020].

Diakow, L.J., Nixon, G.T., Rhodes. R. and van Bui, P. (2006): Geology of the central Toodoggone River map area, north-central British Columbia (parts of NTS 94E/2, 6, 7, 10 and 11); BC Ministry of Energy, Mines and Low Carbon Innovation, Open file map 2006-6, scale 1:50 000, URL <http://cmscontent.nrs.gov.bc.ca/geoscience/PublicationCatalogue/GeoscienceMap/BCGS_GM2006-06.pdf> [September 2020].

Diakow, L.J., Panteleyev, A. and Schroeter, T.G. (1991): Jurassic epithermal prospects in the Toodoggone river area, northern British Columbia: examples of well preserved, volcanic-hosted, precious metal mineralization. Economic Geology, v. 86, p. 529–554.

Diakow, L.J., Panteleyev, A. and Schroeter, T.G. (1993): Geology of the early Jurassic Toodoggone Formation and gold-silver deposits in the Toodoggone river map area, northern British Columbia; BC Ministry of Energy, Mines and Low Carbon Innovation, Bulletin 86, 72 p., URL <http://cmscontent.nrs.gov.bc.ca/geoscience/PublicationCatalogue/Bulletin/BCGS_B086.pdf> [September 2020].

Halley, S. W. (2020): Mapping magmatic and hydrothermal processes from routine exploration geochemical analyses; Economic Geology. V. 115, p. 489–503.

Halley, S.W., Dilles, J.H. and Tosdal, R.M. (2015): Footprints: hydrothermal alteration and geochemical dispersion around porphyry copper deposits; Society of Economic Geologists, Newsletter, no. 100.

Hedenquist, J.W. and Taran, Y.A. (2013): Modeling the formation of advanced argillic lithocaps: volcanic vapor condensation above porphyry intrusions; Economic Geology, v. 108, p. 1523–1540.

Hedenquist, J.W., Arribas, A., Jr. and Reynolds, T.J. (1998): Evolution of an intrusion-centered hydrothermal system: Far Southeast-Lepanto porphyry and epithermal Cu-Au deposits, Philippines: Economic Geology, v. 93, p. 373–404.

Heinrich, C.A. (2007): Fluid-fluid interactions in magmatic-hydrothermal ore formation; Reviews in Mineralogy and Geochemistry, v. 65, p. 363–387.

Heinrich, C.A., Driesner, T., Stefánsson, A. and Seward, T.M. (2004): Magmatic vapor contraction and the transport of gold from the porphyry environment to epithermal ore deposits; Geology, v. 32, p. 761–764.

Kuran, D.L. and Barrios, A. (2005): Geological, geochemical and diamond drilling report on the Sickle-BeeGee Claim Group, Toodoggone area; report prepared for Stealth Mineral Limited, BC Ministry of Energy, Mines and Low Carbon Innovation, Assessment Report 27790A, 28 p., URL <https://aris.empr.gov.bc.ca/ARISReports/27790A.PDF> [November 2020].

Li, Z.X.A., and Lee, C.T.A. (2004): The constancy of upper mantle fO_2 through time inferred from V/Sc ratios in basalts; Earth and Planetary Science Letters, v. 228, p. 483–493.

Loucks, R.R. (2014): Distinctive composition of copper-ore-forming arc magmas; Australian Journal of Earth Sciences, v. 61, no. 1, p. 5–16.

McKinley, B.S.M. (2006): Geological characteristics and genesis of the Kemess North porphyry Au-Cu-Mo deposit, Toodoggone district, north-central British Columbia, Canada; M.Sc. thesis, The University of British Columbia, 136 p., URL <https://open.library.ubc.ca/cIRcle/collections/ubctheses/24/items/1.0052897> [September 2020].

Meyer, C. and Hemley, J.J. (1967): Wall rock alteration; *in* Geochemistry of Hydrothermal Ore Deposits, H.L. Barnes (ed.), Holt, Reinhart and Winston, Inc., New York, New York, p. 166-235.

Panteleyev, A. and Koyanagi, V.M. (1994): Advanced argillic alteration in Bonanza volcanic rocks, northern Vancouver Island – lithologic and permeability controls; *in* Geological Fieldwork 1993, BC Ministry of Energy, Mines and Low Carbon Innovation, BC Geological Survey, Paper 1994-1, p. 101–110, URL <https://www2.gov.bc.ca/gov/content/industry/mineral-exploration-mining/british-columbia-geological-survey/publications/fieldwork> [September 2020].

Pearce, J.A. and Norry, M.J. (1979): Petrogenetic implications of Ti, Zr, Y, and Nb variation in volcanic rocks; Contributions to Mineralogy and Petrology, v. 69, p. 33–47.

Sillitoe, R.H. (1993): Epithermal models: genetic types, geometrical controls and shallow features; *in* Mineral Deposit Modelling, R.V. Kirkham, W.D. Sinclair, R.J. Thorpe and J.M. Duke (ed.), Geological Association of Canada, Special Paper 40, p. 403-417.

Sillitoe, R.H. (2010): Porphyry copper systems; Economic Geology, v. 105, p. 3–41.

Simmons, S.F., White, N.C. and John, D. (2005): Geological characteristics of epithermal precious and base metal deposits; *in* Economic Geology One Hundredth Anniversary Volume 1905–2005, J.W. Hedenquist, J.F.H. Thompson, R.J. Goldfarb and J.P. Richards (ed.), Economic Geology, p. 485–522.

SRK Consulting Inc. (2016): Technical report for the Kemess underground project and Kemess East resource estimate, British Columbia, Canada; report prepared for AuRico Metals Inc., 409 p., URL <https://www.centerragold.com/cg-raw/cg/KemessUG_Updated_Technical-Report_2CA046-004_20160506_FNL.pdf> [September 2020].

Ulusay, R. and Hudson, J.A. (2007): The Complete ISRM Suggested Methods for Rock Characterization, Testing and Monitoring: 1974-2006; compiled by the ISRM Turkish National Group, International Society for Rock Mechanics, ISRM Commission on Testing Methods, 628 p.

van Straaten, B.I and Bouzari, F. (2018): The Middle Jurassic Tanzilla–McBride hydrothermal system: one of the largest lithocaps in BC?; Mineral Exploration RoundUp, Vancouver, BC, January 22–25, 2018, poster presentation.

van Straaten, B.I. and Gibson, R. (2017): Late Early to Middle Jurassic Hazelton Group volcanism and mineral occurrences in the McBride–Tanzilla area, northwest British Columbia; *in* Geological Fieldwork 2016, BC Ministry of Energy, Mines and Low Carbon Innovation, BC Geological Survey, Paper 2017-1, p. 83–115, URL <http://cmscontent.nrs.gov.bc.ca/geoscience/PublicationCatalogue/Paper/BCGS_P2017-01-06_vanStraaten.pdf> [September 2020].

van Straaten, B.I. and Nelson, J.L. (2016): Syncollisional late Early to early Late Jurassic volcanism, plutonism, and porphyry-style alteration on the northeastern margin of Stikinia; *in* Geological Fieldwork 2015, BC Ministry of Energy, Mines and Low Carbon Innovation, BC Geological Survey, Paper 2016-1, p. 113–143, URL <http://cmscontent.nrs.gov.bc.ca/geoscience/PublicationCatalogue/Paper/BCGS_P2016-01-07_vanStraaten.pdf> [September 2020].

van Straaten, B.I., Gibson, R. and Nelson, J. (2017): Preliminary bedrock geology of the Tanzilla and McBride area, British Columbia; BC Ministry of Energy, Mines and Low Carbon Innovation, BC Geological Survey, Open File 2017-9, scale 1:50 000, URL <http://cmscontent.nrs.gov.bc.ca/geoscience/PublicationCatalogue/OpenFile/BCGS_OF2017-09.pdf> [September 2020].

Watanabe, Y. and Hedenquist, J.W. (2001): Mineralogic and stable isotope zonation at the surface over the El Salvador porphyry copper deposit, Chile; Economic Geology, v. 96, p. 1755–1797.